Influence of reaction parameters on nanogold-catalyzed glucose and xylose oxidation: a joint experimental and DFT study

Jay Pee Oña,[†] Laura Laverdure,[‡] Rose Marie Latonen,[†] Narendra Kumar,[†] Markus Peurla,[¶] Ilari Angervo,[§] Karoliina Honkala,[‡] and Henrik Grénman[*,†]

[†]*Faculty of Science and Engineering, Åbo Akademi University, Henriksgatan 2, Turku, FI-20500 Finland*

[‡]*Department of Chemistry, Nanoscience Center, University of Jyväskylä, Jyväskylä, FI-40014 Finland*

[¶]*Institute of Biomedicine, University of Turku, Kiinamyllynkatu 10, Turku, FI-20520 Finland*

[§]*Wihuri Physical Laboratory, Department of Physics and Astronomy, University of Turku, Turku, FI-20014 Finland*

E-mail: henrik.grenman@abo.fi

Abstract

The electrocatalytic oxidation (ECO) of glucose on gold requires alkaline conditions and relatively high potentials ($> 0.3\ V_{RHE}$). Although the adsorption of hydroxide ions (OH_{ads}) is also know to occur under these conditions, the generally accepted proton-coupled electron transfer (PCET) mechanism for sugar ECO does not explicitly state the role of OH_{ads} in the sugar adsorption or oxidation steps. To investigate this, we carried out a combined experimental and density functional theory (DFT) study on

the ECO of glucose and xylose over a nanogold catalyst under temperature and pH control. Grand canonical DFT (GC-DFT) was used to identify the preferred reaction mechanism in which OH_{ads} facilitates the thermodynamically feasible formation of gluconic and xylonic acid. Calculated results also showed that OH_{ads} has a role in improving the acid selectivity. Constant potential electrolyses in sugar solutions were performed using mesoporous (Sibunit) carbon-supported Au nanoparticles (AuNPs) with an average cluster size of 4.7 nm. Experimental results showed that the highest conversions for glucose (57.7 %) and xylose (49.4 %) were obtained at 25 °C and pH 12.5, with gluconic and xylonic acid selectivity of 81.5 % and 87.8 %, respectively. The catalytic activities were high considering the low Au loading ($\sim$ 0.1 % wt.). Higher pH led to a decrease in the ECO rate possibly due to excess hydroxide ions blocking active sites for sugar adsorption. Our results highlight the importance of computational studies in elucidating reaction mechanisms for sugar ECO where sugar acids are the main oxidation products. This is crucial in designing reaction systems for the viable production of these value-added chemicals from biomass.

KEYWORDS: Electrocatalysis, oxidation, glucose, xylose, nanogold, grand canonical DFT

Introduction

The urgent need to replace fossil resources as feedstock for fuel and chemical production is not only due to the detrimental effects their usage has on the environment, but also to their limited availability. The depletion of crude oil is expected to occur within 40 years,[1] and the remaining resources will be mainly allocated towards liquid fuels for air traffic (i.e. jet fuels) and heavy-duty vehicles. Consequently, sustainable technologies harnessing renewable sources of energy (e.g. solar, wind) are currently being developed to meet future energy requirements. A major challenge related to renewable energy sources is their intermittency,

which calls for more effective energy distribution within existing infrastructures or efficient energy storage systems. One strategy is to store renewable energy in the form of chemical bonds. While hydrogen appears to be the best platform chemical for renewable energy storage, its safe transport and efficient storage are obstacles towards its widespread use. Currently, research efforts are devoted to electrochemical syntheses as a possible use for renewable energy. Biomass presents a sustainable platform for electrochemical transformations that could harness renewable electricity to produce value-added chemicals.

Lignocellulosic biomass forms the largest portion of plant biomass and is composed of 25-55 % cellulose, 10-50 % hemicellulose, and 6-30 % lignin.[2,3] It is an attractive feedstock due to its abundance and its utilization for chemical production does not compete with food production. Depolymerization of cellulose and hemicellulose is accomplished by acid hydrolysis in batch or continuous mode and mainly yields glucose, xylose, and mannose.[4–6] These sugars can then be further valorized into higher-value chemicals such as sugar alcohols or sugar acids. For instance, gluconic and xylonic acids produced from the oxidation of glucose and xylose, respectively, are among the top value-added chemicals from biomass[7,8] and are widely employed in the food and pharmaceutical industry. The global market value of gluconic acid in 2020 was $ 1 billion and this value is projected to increase to $1.9 billion by 2028.[9] Xylonic acid shares the market niche as a gluconic acid substitute.[10] Gluconic acid is produced on an industrial scale through a fermentation process aided by *Aspergillus niger* or *Gluconobacter suboxidans* bacteria.[11] High-yield xylonic acid production has been demonstrated using enzymatic catalysis, whole-cell catalysis, and fermentation.[10] Heterogeneous catalytic oxidation of glucose and xylose has been studied using supported noble metal catalysts (Pt, Pd, Au) in the presence of oxygen, air, or hydrogen peroxide as oxidants. Pt-based catalysts demonstrated high activity towards gluconic acid formation, but also formed side products from C-C bond breaking.[12,13] While Pd is less active than Pt,[12] it is normally more selective towards sugar acids.[14] Supported Au catalysts also showed high activities towards glucose oxidation at relatively low temperatures, with selectivity to gluconic acid reaching

up to 100 %.[15]

Electrochemical methods can also be used for sugar oxidation. Electrocatalytic oxidation (ECO) is a non-thermal process that involves the transfer of electrons between the catalyst and the substrate. ECO can be readily carried out in solution at room temperature and pressure and does not require additional oxidative reagents. Glucose and xylose ECO proceeds via a two-electron transfer as shown below:

$$\text{Glucose:} \quad C_6H_{12}O_6 + 3OH^- \rightarrow C_6H_{11}O_7 + 2H_2O + 2e^- \tag{1}$$

$$\text{Xylose:} \quad C_5H_{10}O_5 + 3OH^- \rightarrow C_5H_9O_6 + 2H_2O + 2e^- \tag{2}$$

Au is a well-known catalyst for sugar ECO due to its high activity and resistance to surface poisoning compared to platinum in neutral and alkaline electrolytes.[16] Moggia et al. demonstrated the ECO of glucose over polycrystalline Au into glucaric acid in a two-step cascade reaction providing insight on the influence of reaction conditions.[17] Rafaideen et al.[11] reported a high conversion of glucose (67 %) and xylose (52 %) over a carbon-supported PdAu alloy with high selectivity for gluconic acid (87 %) and xylonic acid (92 %). Mechanistic studies on glucose ECO conducted by Holade et al.[18] showed the high ECO activity over Au under alkaline conditions was due to free or adsorbed hydroxide ions. The exact role of co-adsorbed OH groups in ECO reactions on Au surfaces, however, is still not well understood, given that sugar ECO also occurs on clean Au surfaces at lower potentials (< 0.3 V_{RHE}) as suggested by Adzic et al.[19] Under the currently accepted proton-coupled electron transfer (PCET) mechanism for sugar ECO, the initial adsorption step for the sugar molecule on the catalyst surface is coupled with dehydrogenation and further oxidation on the surface results in the formation of lactone and acid species. An understanding of the relative adsorption energies of reactive species on both clean and hydroxylated Au surfaces would therefore explain the observed enhancement in ECO activity under alkaline conditions.

In this work, we carried out experimental and density functional theory (DFT) studies

to investigate glucose and xylose ECO over a Au catalyst under alkaline conditions. DFT results show the crucial role of co-adsorbed hydroxyl groups in the thermodynamically preferred mechanism which would explain the higher ECO activity and selectivity towards the sugar acid products (i.e. gluconic and xylonic acids) at sufficiently high reaction pH. The nano gold catalyst was prepared from gold sol, the composition of which was previously optimized to produce the cluster size with the highest activity.[20] The catalyst support used was Sibunit carbon, a mesoporous carbon obtained from the pyrolysis of C_1-C_4 hydrocarbons on carbon black powder.[21] Constant-potential electrolyses under pH and temperature control highlighted the effects of these parameters on the overall ECO rates and product selectivity. The results obtained in this study provide crucial information on sugar ECO and demonstrate available electrocatalytic systems for sugar valorization that can potentially harness renewable energy.

Methodological Details

Materials

D-glucose (BioUltra, $\geq$ 98 % wt.) and D-xylose (BioUltra, $\geq$ 99 % wt.) powder reagents were purchased from Sigma Aldrich. Hydrogen tetrachloroaurate (III) hydrate (49 % Au) from Alfa Aesar/ABCR GmbH was used as a metal precursor. Polyvinyl alcohol (PVA, 99+% hydrolysed, MW = 89,000-98,000) from Sigma-Aldrich was used as a stabilizing agent. The catalyst support was Sibunit carbon with physical properties described in our previous work.[20] Carbon felt ($\geq$ 99.0 %, Alfa Aesar) was used to construct the working electrode while microporous meshed fibers of activated carbon (0.60 mm thickness, Kynol®) were used to prepare the counter electrode. All other chemicals used were of analytical grade. Chemical solutions were prepared using deionized water (resistivity 18 MΩ-cm).

Catalyst preparation

The catalyst was prepared by immobilizing preformed AuNPs from gold sol onto the mesoporous (Sibunit) carbon support. To prepare the gold sol, 1.25 mL of 2 % wt. PVA solution was added to 165 mL of 60 µg mL^{-1} $HAuCl_4$ solution under constant stirring, which corresponds to a PVA/Au weight ratio of 5. Thereafter, 1.0 mL of 0.1 M $NaBH_4$ solution was added dropwise to the mixture, which resulted in a bright orange solution. After two minutes of continuous stirring, 0.5 g of Sibunit carbon was added to the solution to obtain a nominal metal loading of 1 % wt. The catalyst slurry was stirred overnight (16 h) and subsequently filtered under vacuum. The filtered catalyst was then washed thoroughly with hot (90 °C) deionized water to remove the excess PVA. The sibunit carbon-supported Au (SC/Au) catalyst was then dried overnight in an oven at 60 °C.

Catalyst characterization

The physico-chemical properties of the SC/Au catalyst were studied using nitrogen physisorption, scanning electron microscopy/energy dispersive X-ray analysis (SEM/EDXA), transmission electron microscopy (TEM), inductively coupled plasma-optical emission spectrometry (ICP-OES) and X-ray diffraction (XRD). Nitrogen physisorption was used to estimate the specific surface area and pore volume using MicroActive 3Flex^{TM} 3500 (Micromeritics) sorptometer. The surface morphology and Au content were obtained from SEM/EDXA using a Leo Gemini 1530 scanning electron microscope with a Thermo Scientific UltraDry Silicon Drift Detector. The Au nanoparticle sizes and distribution were determined from TEM using JEOL JEM 1400 Plus transmission electron microscope operating at 120 kV acceleration voltage and 0.38 nm resolution. Crystallographic data was obtained from XRD analysis using a PANalytical Empyrean diffractometer.

Electrochemical measurements

Electrochemical measurements were carried out on a thermostated, single-compartment, three-electrode cell connected to a Gamry (Reference 620) potentiostat. Potentials were measured against an Ag/AgCl/3M KCl (Thermo Scientific Orion^{TM} 900100) reference electrode. The working electrode was constructed by infiltrating the catalyst ink on a carbon felt substrate (9 cm^2 geometric area, Alfa Aesar). The catalyst ink was prepared by suspending 10 mg of the SC/Au catalyst in 938 µL deionized water and adding 125 µL of Nafion 117 thereafter. The catalyst mixture was then thoroughly mixed and deposited dropwise on the carbon felt, and dried overnight at room temperature. The counter electrode (9 cm^2 geometric area) was constructed by attaching an activated carbon cloth (0.60 mm thickness, Kynol®) to a carbon rod (99.999 % carbon, Strem Chemicals Inc.) using carbon glue (Electrodag® PF-407C). Measurement of the electrochemical surface area (ECSA) of gold was carried out using cyclic voltammetry in 0.1 M NaOH at 20 mV s^{-1}.[22]The charge from the reduction of gold oxide was determined from the cathodic peak at ca. 1.0 V_{RHE} (see Figure SI-1). The ECSA was derived from this charge, using a charge density of 386 µC cm^{-2}, which corresponds to the reduction of a monolayer of gold oxide. In all experiments, the working solution was purged with nitrogen gas before the measurements and a supply of N_2 was kept above the liquid's surface during analysis.

Electrocatalytic oxidation of glucose and xylose

Constant-potential electrolyses were conducted using the single-compartment, three-electrode electrochemical cell to study the influence of reaction temperature and pH on the electrooxidation of glucose and xylose. The applied potential during temperature and pH studies was +1.3 V_{RHE} to provide sufficient potential for appreciable sugar oxidation while avoiding the oxidation of Au to the oxide form. To investigate deactivation of the Au catalyst, a potential-programmed method for sugar electrolysis, previously developed by Belgsir et al.[23] was employed. The potential cycle consisted of potential steps at 0.13 V_{RHE}, 1.33 V_{RHE},

and 1.93 V_{RHE} applied to the anode for 10 s, 30 s, and 5 s, respectively, throughout the ECO period. A higher potential step at 1.93 V_{RHE} would desorb any adsorbed species on the catalyst surface as gold is oxidized to $Au(O)_x$ species. At the potential step at 0.13 V_{RHE}, the $Au(O)_x$ species are reduced to the metallic Au^0 onto which sugar molecules could adsorb. This is then followed by oxidation of the sugar molecules at 1.33 V_{RHE}. This potential cycle allowed for continuous generation of a metallic gold surface for long periods of reaction. The reaction temperature was maintained using a thermostat during electrolysis while the pH was kept constant by the addition of 1 M NaOH or 1 M HNO_3 using an automatic titrator (Metrohm 799 GPT Titrino) equipped with a pH sensor. Mass transfer was facilitated by stirring the reaction solution magnetically at 600 rpm.

The influence of pH on sugar conversion and selectivity was studied at 25 °C as the highest productivity of sugar acids with appreciable selectivity was observed at this temperature. ECO experiments were done using 0.1 M glucose or xylose in 0.1 M (pH 12.5) or 1 M (pH 13.5) NaOH as supporting electrolyte. Solutions at pH 11 were obtained by adding an appropriate amount of 2 M HNO_3 to the solution of 0.1 M glucose or xylose in 0.1 M NaOH, to maintain the conductivity of the working solution. Using concentrated H_2SO_4 for pH adjustment is not advisable as SO_4^{2-} ions adsorb on gold surfaces and block the reacting species.[24–26]

Electrolyses were carried out for a maximum of 6 h and samples were taken at different times during the experiments. Samples were immediately neutralized to pH 7 using concentrated H_2SO_4. Reaction products were analyzed using HPLC with an Aminex HPX-87C column and refractive index detector. The mobile phase was 1.2 mM $CaSO_4$ at 0.3 mL min^{-1} flowrate and the column temperature was 50 °C. The HPLC instrument was calibrated using high purity standards (glucose, xylose, fructose, xylulose, gluconic acid, glucaric acid, xylonic acid) purchased from Sigma Aldrich.

Computational details

The sugar-based molecules considered include the acyclic, α-, and β-pyranose forms of glucose and xylose, the corresponding lactones, gluconate, gluconic acid, xylonate, and xylonic acid. The furanose forms of glucose and xylose are neglected as they are only found in trace amounts in solution.[27–29] Given the possibility of glucose and xylose isomerizing to form fructose and xylulose, respectively, the anomers of each (linear, α-, and β-furanose for fructose and xylulose as well as the α- and β-pyranose for fructose) were also considered. Au(111) was used to model the gold nanoparticle's catalytic surface. The Au(111) surface was constructed as a periodic, 3-layer, 4×4 orthogonal cell with approximately 20 Å of space separating the slabs. These dimensions were selected to minimize computational expense as well as image interaction. The longest sugar-based molecule has at least 3 Å (approximately the length of a hydrogen bond) separating it from its translational image should the molecule adsorb parallel to the surface. The bottom layer of the Au(111) slab was fixed to bulk positions while the top two layers were allowed to relax. Previous grand canonical DFT (GC-DFT) studies have shown that a 1/3 – 1/2 ML coverage of OH exists on the Au(111) surface at high pH and applied potential but that a 1/6 ML OH was sufficient to capture the effects of adsorbed OH on glycerol oxidation.[30] Here, we use a 1/4 ML OH to accommodate the larger surface area produced by a 4×4 supercell. Five symmetrically unique 1/4 ML OH configurations were optimized. The lowest energy configuration was selected to model the hydroxylated Au(111) surface.

The sugar-based molecules can adopt many configurations as adsorbates and in solution corresponding to local minima on their respective potential energy surfaces. The DockOnSurf software[31] was used to generate candidate configurations of each molecule in solution as well as adsorbed on the bare and hydroxylated Au(111) surfaces. Given the large number of configurations created for each molecule, the initial structures underwent a filtering process (see Figure 1 and the Supporting Information for further details) to identify the most likely minimum energy configuration.

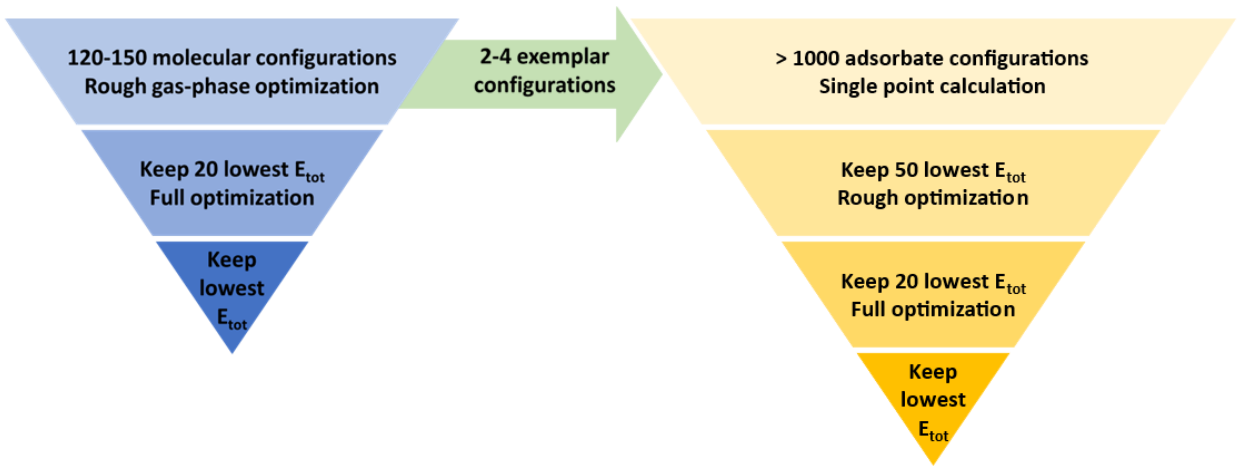

Figure 1: Structural filtering process for solution phase molecules and adsorbates. Configurations are ranked and selected based on their total energies.

All calculations were carried out using the GPAW 21.6.0 software.[32,33] Systems involving the Au(111) surface were fully optimized with GC-DFT[34] using the solvated jellium model[35] to achieve implicit water solvation and a target potential of 4.44 V_{abs}. A 4×4×1 k-point grid was used for all surfaces. Solution phase molecules, which are assumed in the bulk solution, were fully optimized with 'canonical' DFT in a non-periodic cell with 20 Å of continuum solvent model[36] water in each direction. The gamma point was used to determine the electronic structure of solution phase molecules All molecules, surfaces, and adsorbates were optimized using PBE-DFT[37] with a 0.18 Å spaced grid-based basis set and the TS09 dispersion correction.[38] The combination of a GGA functional and dispersion correction such as PBE+TS09 combines computational efficiency with the ability to account for van der Waals interaction and has been successfully used in similar contexts.[30,39] The error in total and adsorption energies due to the implicit solvent model is expected to be ∼0.2 eV.[40] While this error may appear significant, its importance is diminished when examining relative energies and trends. Furthermore, an implicit solvent model improves upon gas-phase results by mimicking ensemble effects and giving more accurate adsorption geometries which is important for surface reactions.[40]

The calculated lattice constant for Au is 4.140 Å, in good agreement with the experimen-

tal value of 4.065 Å.[41] The Fermi level (E_F) is related to the electrode's absolute potential and can be converted to the SHE scale through $U_{SHE} = -e(E_F + 4.44eV)$. The Fermi level was found to be -4.82 eV for both bare and hydroxylated Au(111) surfaces. Sugar adsorption has a negligible effect on the E_F. The electrode potentials are therefore 1.03 V_{RHE} (pH = 11), 1.12 V_{RHE} (pH = 12), and 1.15 V_{RHE} (pH = 13).

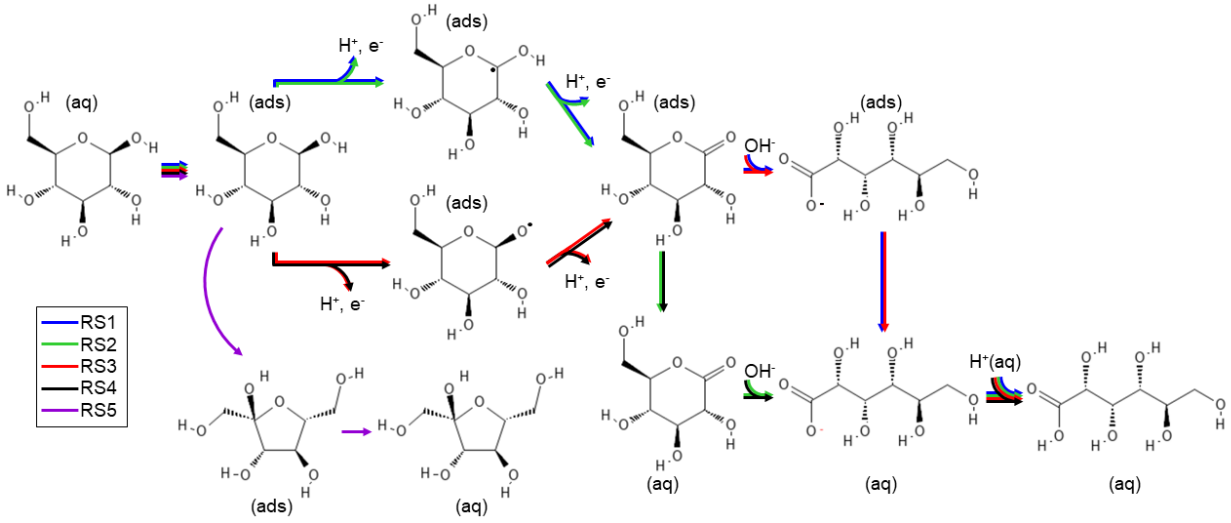

Figure 2: General mechanism for sugar oxidation shown for β-D-glucose. All steps are assumed to occur at the same pH except the final acid formation which occurs at lower pH. Similar steps are taken for α-D-glucose as well as α- and β-D-xylose.

Adsorption energies were calculated according to

$$E_{ads} = E_{mol*} - E_{mol} - E_* \tag{3}$$

where E_*, E_{mol}, and E_{mol*} represent the energy of the surface, the solution phase molecule, and the adsorbed molecule, respectively. The general mechanism followed for both α and β anomers of both glucose and xylose and on which the corresponding reaction potential energy surfaces are based is shown in Figure 2. The explicit equations are given in the Reaction energy profiles section of the Supporting Information. The relative populations were determined using

$$\frac{e^{-E_j/kT}}{\sum_{i=1}^{N} e^{-E_i/kT}} \tag{4}$$

where E_i and E_j are relative energies with respect to the most stable configuration, k is the Boltzmann constant and T is 298.15 K. The potential dependency of the reactions' thermodynamics is described using the standard equilibrium potential (U_{eq}^{0}), surface equilibrium potential (U_{eq}^{surf}), and limiting potential (U_L). These potentials are defined as follows

$$U_{eq,RHE}^{0} = \Big[\sum_i \Delta E_i(aq)(U_{RHE} = 0)\Big]/N_{e,tot} \tag{5}$$

$$U_{eq,RHE}^{surf} = \Big[\sum_i \Delta E_i^{*}(U_{RHE} = 0)\Big]/N_{e,tot} \tag{6}$$

$$U_L = \max\{\Delta E_i(U_{RHE} = 0)\} \tag{7}$$

where the index i refer to an electrochemical step, * refers to an adsorbed species, and $N_{e,tot}$ represents the net number of electrons transferred. A potential of 1.30 V_{RHE} is also included to compare the effects of the applied potential with the experimental results. The pH effects are included by using the RHE scale.

Results and discussion

Catalyst characterization

The TEM image of the SC/Au catalyst in Figure 3a shows the Au nanoparticles are randomly distributed crystals on the mesoporous carbon support. The particle size histogram in Figure 3b shows a narrow distribution with an average particle size of 4.7 ± 1.1 nm. The Au dispersion (D_{Au}) determined from the Au particle size was 24.9 %, and the exact calculation is described in the Supporting Information. The diffractogram of the SC/Au catalyst (Figure 4) shows peaks close to 38°, 44°, 65°, and 78°, which are representative of fcc gold. On the other hand, the broad peak close to 25° corresponds to the carbon support.

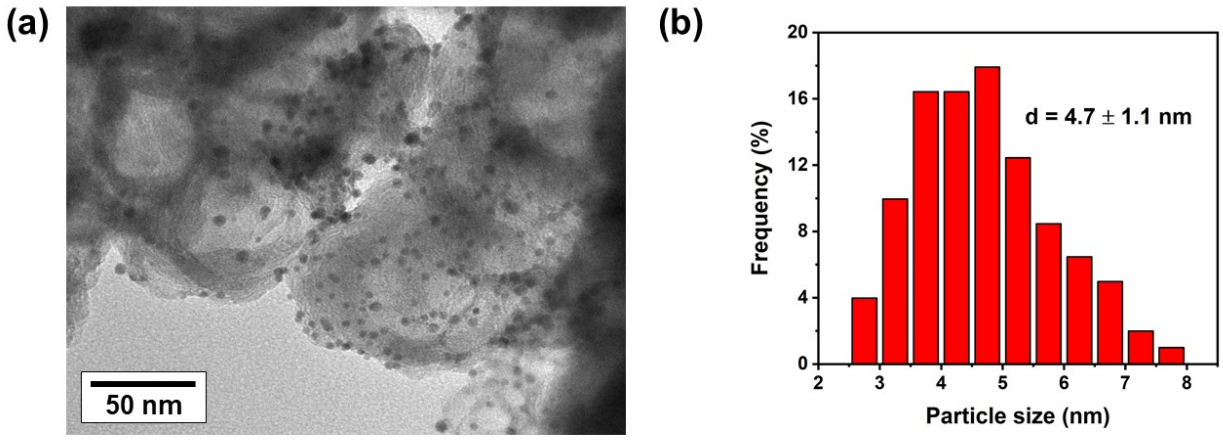

Figure 3: TEM image (a) and particle size distribution of AuNPs (b) of the SC/Au catalyst.

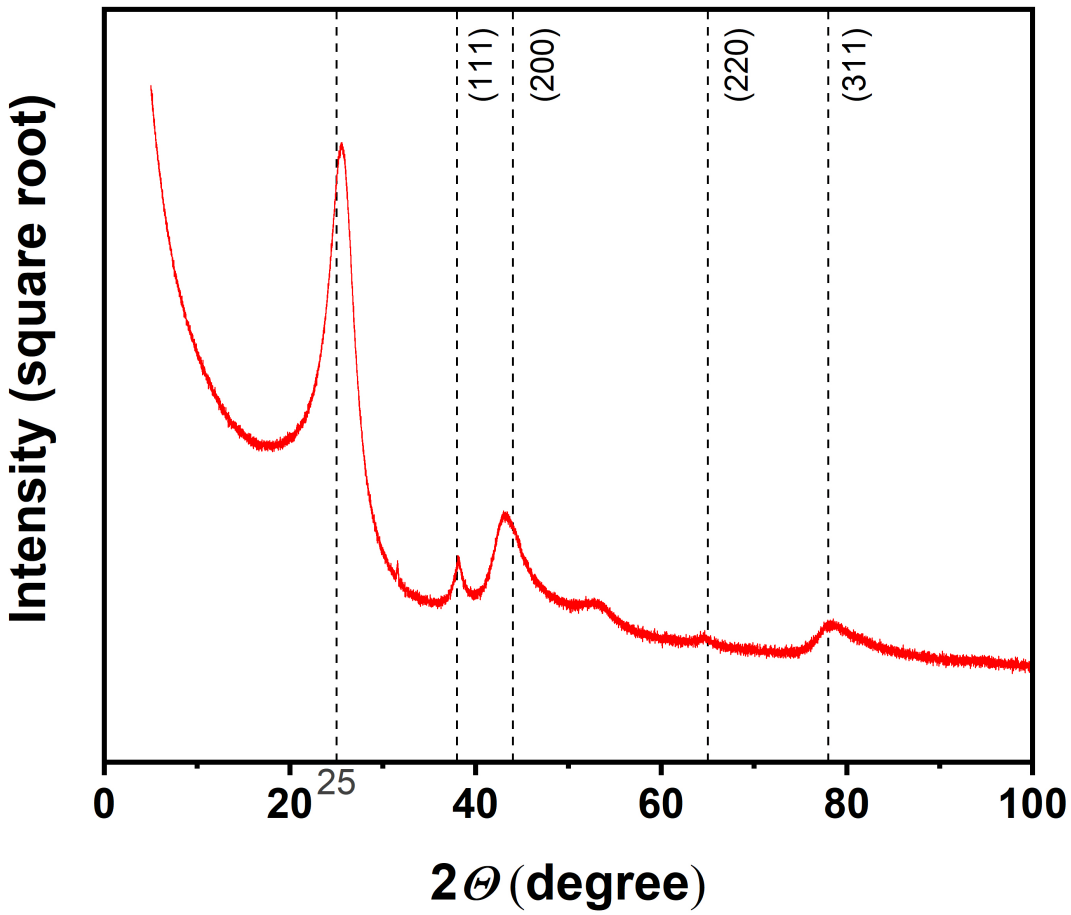

Figure 4: X-Ray diffraction pattern of the SC/Au catalyst.

Surface area values and other physical measurement results are summarized in Table 1. The specific surface area determined from N_2 physisorption was 226 m^2g^{-1} with a pore volume of 0.48 cm^3g^{-1}. The Au loading obtained from ICP-OES was 0.10 % wt., which was significantly lower than the nominal loading of 1 % wt. This is attributed to the weaker interaction of AuNPs with the surface groups of the carbon support and the high stability of the Au sol. Based on the geometric area of the working electrode (9 cm^2), the actual loading was 1.1 μg_{Au} cm^{-2}. The electrochemically active surface area (ECSA) was estimated from the charge of $Au(O)_x$ reduction[20,22] and was calculated to be 0.24 m^2g^{-1}.

Table 1: Physico-chemical measurement data for the SC/Au catalyst.

Au Loading ($\mu g_{Au} cm^{-2}$)	Average Size (nm)	Au Dispersion (%)	Specific Surface Area (m^2g^{-1})	Pore Volume (cm^3g^{-1})	ECSA (m^2g^{-1})	TEM-based specific area of Au (m^2g^{-1})
1.1	4.7±1.1	24.9	226	0.48	0.24	0.07

Electrocatalytic oxidation of glucose and xylose

The cyclic voltammograms recorded for the SC/Au catalyst in glucose (Figure 5a) and xylose (Figure 5b) solutions resemble a typical voltammogram for sugar electrooxidation over polycrystalline[17,42,43] and supported gold catalysts[44] in an alkaline medium. The oxidation of glucose and xylose is indicated by the increase in anodic current in the forward scan starting at ca. 0.5 V_{RHE} and reaching an oxidation peak in the forward scan at ca. 1.5 V_{RHE} for both sugars. Previous studies on glucose electrooxidation suggest that the oxidation peak at 1.5 V_{RHE} is due to glucose oxidation processes that produce gluconate.[42] Our previous investigation on sugar oxidation over similarly prepared SC/Au catalysts showed that glucose and xylose oxidation occur as early as 0.9 V_{RHE}.[20] Adzic et al.[19] proposed that glucose oxidation at lower potentials (0.0 to 0.6 V_{RHE}) would involve metallic Au with no coadsorbed hydroxide (OH_{ads}), while at higher potentials, the oxidation would coincide with the

formation of $Au(OH)_x$ species. Based on in-situ FT-IR voltammetric measurements, Holade et al.[18] proposed a general mechanism for glucose electrooxidation as a function of applied potential. At lower potentials (< 0.3 V_{RHE}) the adsorption of glucose is coupled with the dehydrogenation of the anomeric carbon followed by the formation of adsorbed gluconolactone. The gluconolactone desorbs from the surface and hydrolyzes into gluconate in alkaline medium. At higher potentials (> 0.3 V_{RHE}) where $Au(OH)_x$ species are present, this adsorbed gluconolactone either desorbs or undergoes self-rearrangement to form an adsorbed gluconate. Above 1.5 V_{RHE}, a decrease in anodic current was observed in both glucose and xylose solutions (Figure 5) due to the oxidation of gold to $Au(O)_x$ which is not active towards sugar oxidation.[44] As the potential increases, the oxidized sugar species desorb from the surface of the electrode.

In the backward scan, another oxidation peak can be seen for both sugars at ca. 1.3 V_{RHE}. This peak is associated with the oxidation of sugars over regenerated Au surfaces formed from the reduction of $Au(O)_x$.[18,42] Pasta et al. suggested that the glucose oxidation peak in the reverse scan was would have lower intensity than the oxidation peak in the forward scan as some of the active sites may still have adsorbed gluconate.[42] The oxidation peak in the reverse scan shown in Figure 5 was lower in intensity for xylose oxidation than for glucose. This would indicate that oxidation products from xylose are more strongly adsorbed than those from glucose as observed by Rafaideen et al.[11]

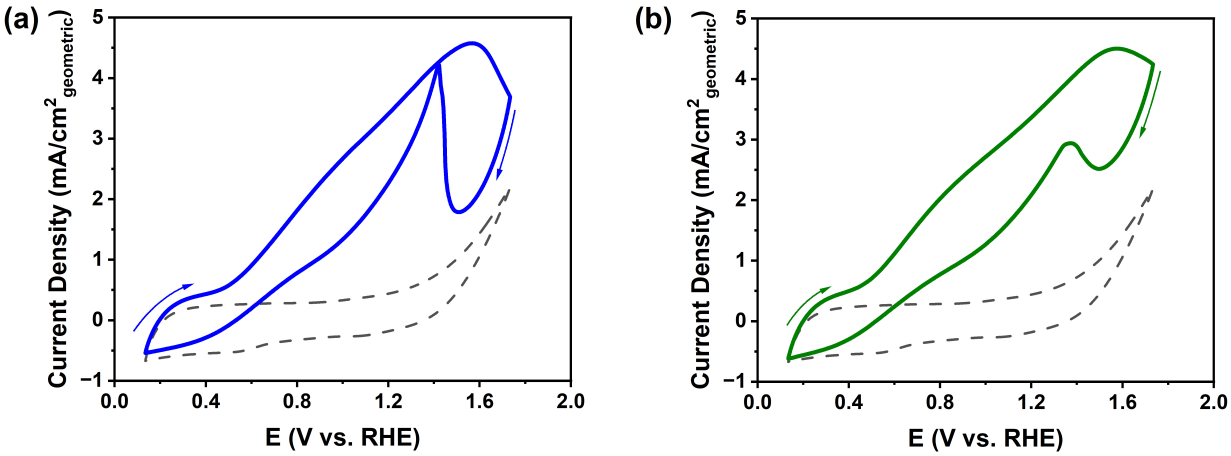

Figure 5: Cyclic voltammograms recorded for the SC/Au catalyst in 0.1 M glucose (a) and in 0.1 M xylose (b) with 0.1 M NaOH supporting electrolyte. Scans recorded in the pure supporting electrolyte are represented by dashed curves in both figures. The scan rate used was 10 mV s^{-1}.

Temperature effects

Glucose and xylose ECO was studied at different temperatures (T= 5-40 °C). Cyclic voltammograms recorded in the sugar solutions show anodic peak current density increasing with increasing temperature (Figure SI-16) as observed earlier by Yei et al.[45] The Arrhenius kinetic theory enables the determination of the electrochemical activation energy E_a using experimental data according to Equation 8:[46,47]

$$E_a = R\frac{\mathrm{d}(\ln I)}{\mathrm{d}(1/T)} \tag{8}$$

where R refers to the universal gas constant (8.314 J $mol^{-1}K^{-1}$), while I and T correspond to current and temperature, respectively. Using the voltammetric data, E_a was evaluated at different oxidation potentials (E_{ox}) applied for glucose and xylose. As shown in Figure SI-17, the E_a value varied depending on E_{ox}. A similar polynomial trend for the E_a value as a function of E_{ox} was also observed for the electrooxidation of glucose at pH 7.4,[48] which is consistent with theoretical calculations carried out by Protsenko and Danilov.[49] In the present study, the E_a values obtained for glucose ECO ranged from 8 to 22 kJ mol^{-1}, while those for xylose ranged from 13 to 24 kJ mol^{-1}. The low E_a values (<50 kJ mol^{-1})

indicate that the kinetics for glucose and xylose oxidation are largely governed by diffusion processes.[17,46,50,51]

Long-term electrolyses at a constant potential of 1.3 V_{RHE} were carried out to study the bulk conversion and selectivity of glucose and xylose ECO. The conversion of glucose increased with higher reaction temperatures reaching 64.6 % at 40 °C (Table 2). However, the increase in reaction temperature was accompanied by the increased formation of fructose as shown in Figure 6b, from the base-catalyzed isomerization of glucose. Higher reaction temperatures also promoted the formation of other oxidative degradation products from glucose (glycolic, oxalic, formic, and tartaric acid), which decreased the selectivity towards gluconic acid formation as shown in Table 2. There was a large increase in TOF and productivity of gluconic acid from 5 °C (2359 h^{-1}) to 25 °C (4300 h^{-1}), but only a minimal increase at 40 °C (4486 h^{-1}). This is largely due to the increased formation of by-products at 40 °C, which decreased the number of available glucose molecules for oxidation.

For xylose ECO, higher reaction temperatures also increased conversion (Figure 6c) but at the expense of selectivity towards xylonic acid production (Figure 6d). At 40 °C, more side products were formed from xylose ECO compared to glucose ECO. These include formic acid, acetic acid, and glycolic acid among other degradation products as analyzed by NMR spectroscopy. The TOF and xylonic acid productivity were lower at 40 °C (1397 h^{-1}, 0.118 mol m^{-2}_{ECSA} h^{-1}) than at 25 °C (1897 h^{-1}, 0.160 mol m^{-2}_{ECSA} h^{-1}) due to extensive formation of by-products.

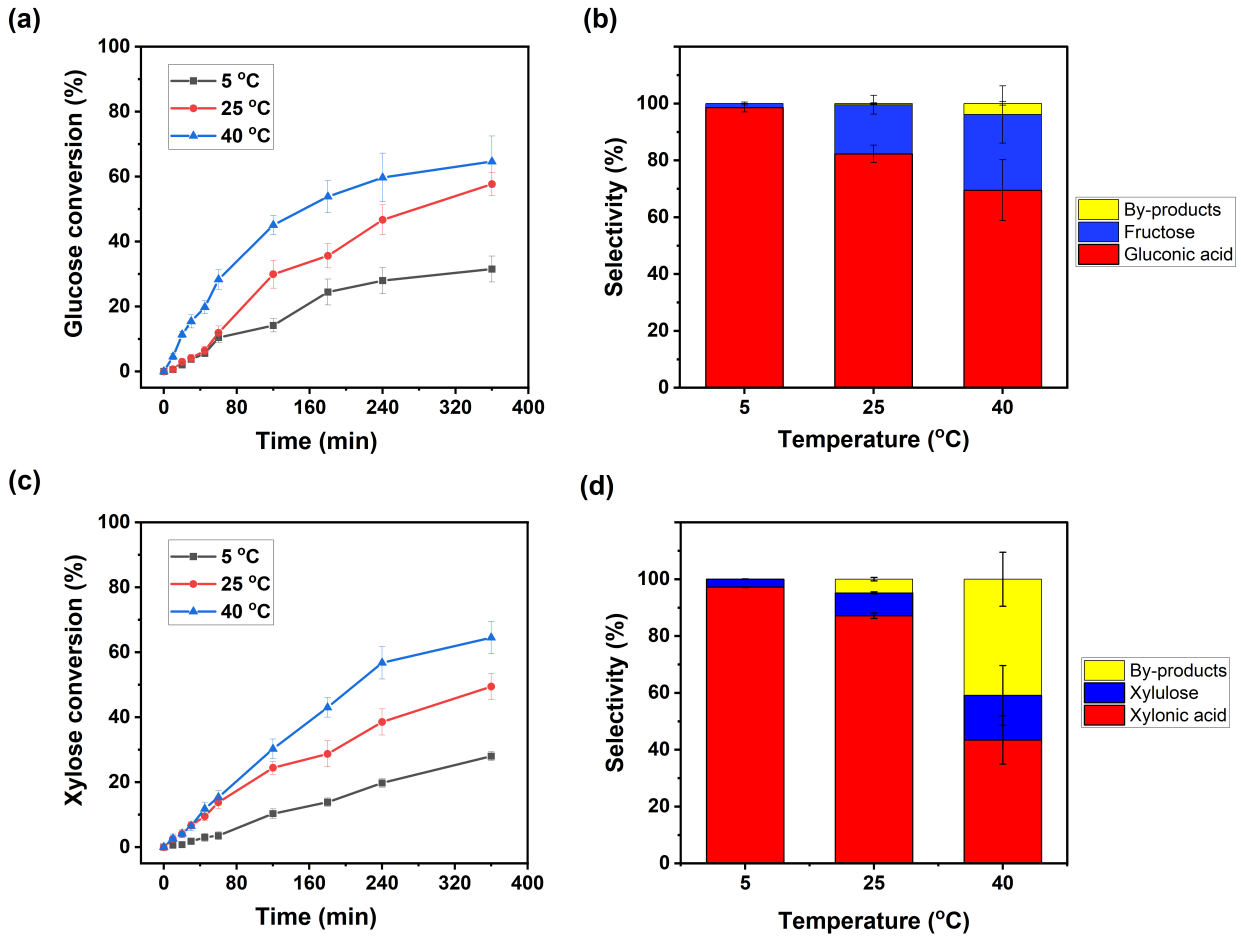

Figure 6: Time-dependent conversion of glucose (a) and xylose (c) at different temperatures for ECO over the SC/Au catalyst and corresponding selectivity to gluconic acid (b) and xylonic acid (d) compared to other reaction by-products. Electrolyses were carried out at an applied potential of 1.3 V_{RHE} in 0.1 M of glucose and xylose with 0.1 M NaOH (pH = 12.5) for 6 h. The reaction solution was stirred at a rate of 600 rpm.

Table 2: Summary of results obtained from the ECO of glucose and xylose at different reaction temperatures. Electrolyses were carried out at an applied potential of 1.3 V_{RHE} for 6 h in 0.1 M of sugar with 0.1 M NaOH as supporting electrolyte (pH 12.5).

Sugar	Temperature °C	Conversion (%)	Acid Selectivity (%)	Acid TOF (h^{-1})	Acid Productivity (mol $m^{-2}_{ECSA} h^{-1}$)
glucose	5	31.5±3.5	98.6±1.5	2359	0.200
	25	57.7±3.5	81.5±4.2	4300	0.364
	40	64.6±7.9	69.5±10.7	4486	0.380
xylose	5	28.0±1.3	97.2±0.5	1091	0.092
	25	49.4±3.5	87.8±0.9	1897	0.160
	40	64.5±5.0	43.5±8.5	1397	0.118

From the experimental data, it can be concluded that while sugar ECO at lower temperatures (5 °C) would result in higher selectivity towards gluconic acid (98.6 %) or xylonic acid (97.2 %), higher temperatures are required to achieve appreciable yields and conversion rates. However, as observed in this work and earlier studies on glucose ECO,[17] higher temperatures give rise to side products that decrease the overall ECO rate and product selectivity. Many of these side reactions, such as the isomerization of glucose and xylose into fructose and xylulose, respectively, occur in the bulk solution. Comparing the TOF values at 5 °C where minimal side reactions were observed, the rate of gluconic acid formation (2359 h^{-1}) was significantly higher than that for xylonic acid (1091 h^{-1}). This would indicate that glucose has a higher reactivity than xylose towards ECO over the SC/Au catalyst.

pH effects

As shown in Figure 7a, glucose conversion increased as the pH increased from pH 11 (7.4 %) to pH 12.5 (57.7 %) and then decreased as pH increased further to pH 13.5 (25.4 %). Despite high concentrations of hydroxide, the selectivity towards gluconic acid formation was lower at pH 13.5 (11.9 %) than at pH 12.5 (81.5 %) (Table 3). A similar trend in pH effects was observed for xylose ECO, where the highest conversion and selectivity was obtained at pH 12.5 (Figure 7c and Table 3). A suitably high concentration of OH^- is necessary for sugar electrooxidation as observed for glucose,[18,24,52–54] which would explain

the higher conversion and sugar acid selectivity at pH 12.5 than at pH 11. However, a very high concentration of OH^- could hinder glucose and xylose adsorption by decreasing the number of active bare Au sites on the surface,[52] which would explain the lower conversion at pH 13.5. Tung et al. attributed the decrease in activity to the passivation of the Au surface caused by the formation of Au(O)x,[55] while Pasta et al. cited the oxidation of Au surfaces to $Au(OH)_3$ for the catalyst's deactivation at higher potentials.[42] To probe this, we conducted a potential-programmed method for sugar electrolysis described in section 2.2 that continuously reduced Au to the metallic state. Figure SI-18 compares sugar ECO using a fixed (static) potential and potential cycling. For glucose ECO, the conversion after 6 h of potential-programmed electrolysis was 46.6 % with a gluconic acid selectivity of 76.1 %. This was lower than the glucose conversion of 57.7 % using a fixed potential mode, which also had a higher selectivity for gluconic acid (81.5 %). Similarly, the conversion of xylose and xylonic acid selectivity were lower for the potential programmed ECO (41.0 % and 75.8 %, respectively) than for the static-potential ECO (49.4 % and 87.8 %, respectively). This would indicate that there is no significant deactivation of the Au catalyst at the working potential (+1.3 V_{RHE}) throughout the reaction. Therefore, the decreased formation of sugar acids at higher pH can be attributed to the competitive adsorption of OH^- ions on the Au surface.

Table 3: Summary of results obtained from the ECO of glucose and xylose at different pH conditions. Electrolyses were carried out at an applied potential of 1.3 V_{RHE} for 6 h in 0.1 M of sugar at 25 °C.

Sugar	pH	Conversion (%)	Acid Selectivity (%)	Acid TOF (h^{-1})	Acid Productivity (mol $m^{-2}h^{-1}$)
glucose	11.0	7.4±3.0	32.9±3.0	169	0.014
	12.5	57.7±3.5	81.5±4.2	4300	0.364
	13.5	25.4±7.5	11.9±1.5	209	0.018
xylose	11.0	11.1±3.5	38.5±3.0	344	0.029
	12.5	49.4±3.5	87.8±0.9	1897	0.160
	13.5	22.7±4.0	10.5±1.0	158	0.013

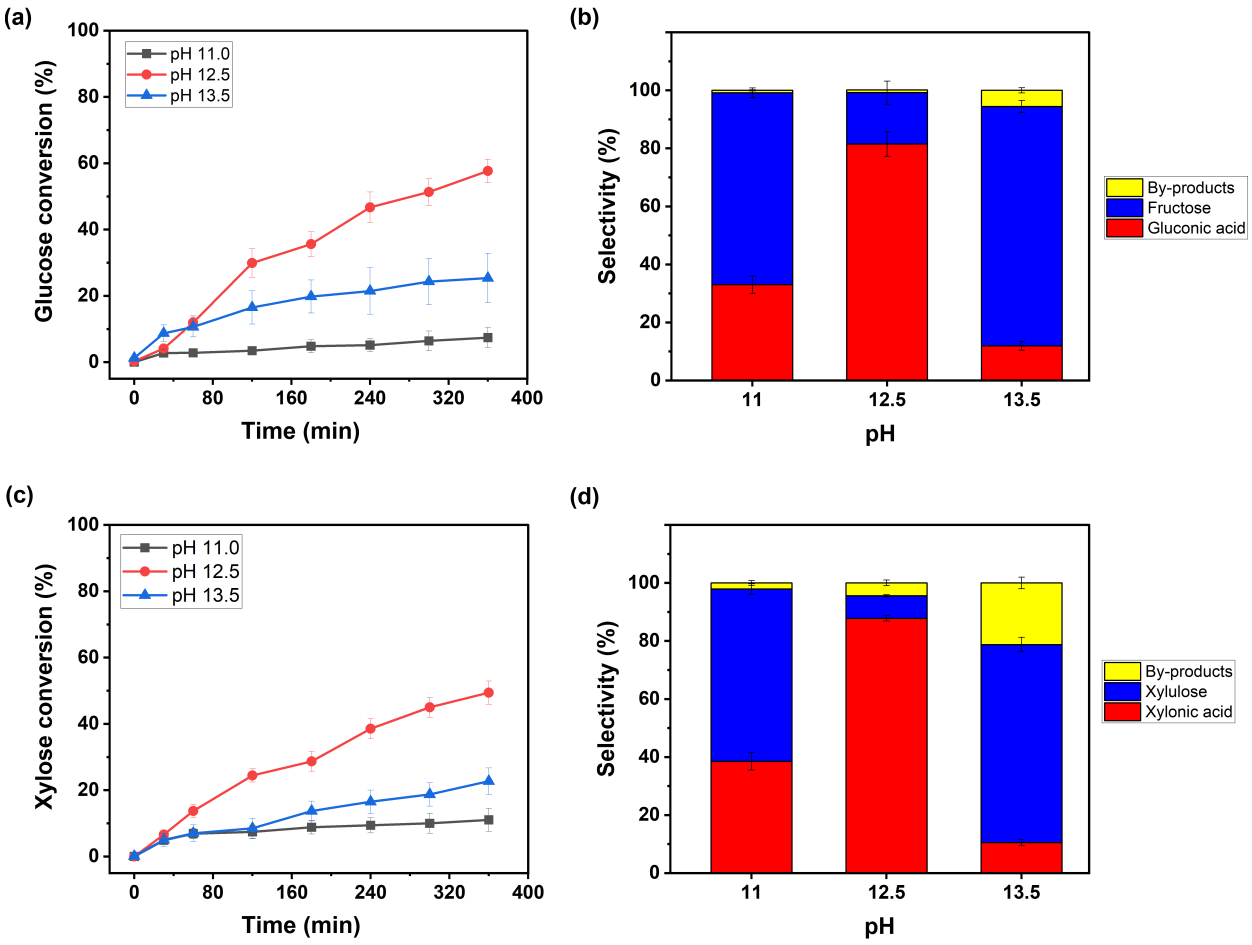

Figure 7: Time-dependent conversion of glucose (a) and xylose (c) at different pH conditions for ECO over the SC/Au catalyst and corresponding selectivity to gluconic acid (b) and xylonic acid (d) compared to other reaction by-products. Constant-potential electrolyses were carried out at 1.3 V_{RHE} for 6 h using 0.1 M glucose and xylose at 25 °C. The reaction solution was stirred at a rate of 600 rpm.

In addition to lower selectivity towards gluconic and xylonic acid, higher pH also leads to degradation products from glucose and xylose. These mostly include lower molecular weight carboxylic acids, which were formed more extensively during xylose ECO than during glucose ECO (Figure 7b and 7d). This would indicate that xylose has a higher propensity towards C-C bond breaking than glucose, especially under more alkaline conditions, possibly in the bulk solution as well as on the surface of the catalyst.

Simulated pH effects

Table 4: Energies (eV) and relative populations (%) of glucose and xylose. Relative energies are given for solution phase sugars and adsorption energies are given for the clean and hydroxylated Au(111) surface. Relative populations are given in parentheses.

Sugar	Solvated		Au(111)		Au(111) + 1/4 ML OH	
D-glucose	0.30	(6×10^{-4})	−1.07	(4×10^{-5})	−1.41	(6×10^{-9})
β-D-glucopyranose	0.00	(69.48)	−1.15	(99.55)	−1.52	(0.05)
α-D-glucopyranose	0.02	(30.52)	−1.03	(0.45)	−1.73	(99.95)
D-fructose	0.12	(0.54)	−0.96	(6.03)	−1.20	(2×10^{-7})
β-D-fructopyranose	0.00	(53.52)	−0.87	(15.47)	−1.36	(0.01)
α-D-fructopyranose	0.02	(27.17)	−0.78	(0.26)	−1.36	(0.01)
β-D-fructofuranose	0.05	(6.45)	−0.94	(33.00)	−1.53	(1.03)
α-D-fructofuranose	0.04	(12.33)	−0.93	(45.24)	−1.63	(98.95)
D-xylose	0.22	(0.01)	−0.65	(4×10^{-7})	−1.17	(1×10^{-8})
β-D-xylopyranose	0.02	(34.18)	−0.94	(99.99)	−1.55	(100)
α-D-xylopyranose	0.00	(65.81)	−0.68	(0.01)	−1.24	(1×10^{-3})
D-xylulose	0.05	(13.28)	−0.78	(1.05)	−1.13	(8×10^{-6})
β-D-xylulofuranose	0.00	(80.18)	−0.85	(91.41)	−1.51	(99.99)
α-D-xylulofuranose	0.06	(6.55)	−0.85	(7.54)	−1.34	(0.01)

The relative populations of solvated glucose tautomers (see Table 4) are in good agreement with experimental values.[27] Although our calculated relative populations of solvated xylose tautomers are in contradiction with experimental results, they agree with previous computational studies.[28,29] The calculated relative populations of fructose and xylulose tautomers also differ from experimental values.[56–59] Nevertheless, qualitative trends are retained, namely the β-pyranose tautomer of both fructose and xylulose has the highest population while the acyclic form has the lowest. The discrepancy between computational and experi-

mental populations of sugar tautomers has previously been attributed to solvent rearrangement around the sugar.[28] Explicit solvation would correct this; however, such calculations are costly computationally and beyond the scope of the present study.

The adsorption energies given in Table 4 show that the β-pyranose form of glucose and xylose is preferentially adsorbed over the α-pyranose and acyclic forms on the clean Au(111) surface. Although acyclic fructose has the most exothermic adsorption energy, the relative energies of adsorbed fructose tautomers on bare gold suggest that α- and β-fructofuranose will be in higher concentration on a clean Au(111) surface. Similarly, for xylulose, both cyclic forms have the same adsorption energy, but the relative energies favor a higher β-xylulofuranose population.

All sugars are very sensitive to the orientation of the alcohol groups with respect to the surface, particularly towards coadsorbed hydroxyl groups (see Figure 8 and Figures S4-S7 for adsorbed structures). Certain configurations of glucose and xylose cause the deprotonation of alcohol groups not involved in the formation of the lactone and sugar acid. The alcohol group transfers its proton to a coadsorbed hydroxyl group, thus forming an adsorbed water molecule. Similar observations were made for the structures of the first intermediate leading to the lactone. These deprotonated configurations may also be considered as intermediates towards other products, however the mechanisms and final products resulting from these configurations are unknown. To preserve the molecular identity of the adsorbates considered as well as the surface pH through the number of adsorbed hydroxides, these dissociated structures are excluded from further consideration. Thus, considering only intact sugar molecules, the tautomers of fructose, xylose, and xylulose with the highest population on clean Au(111) also have the lowest adsorption energies and are enriched on the Au(111) + 1/4 ML OH surface. In contrast, α-D-glucopyranose adsorption becomes more exothermic than β-D-glucopyranose on the hydroxylated surface. The relative populations of α- and β-glucopyranose are also reversed compared to the clean Au(111) surface. Regardless of tautomerism, the adsorption energy becomes more exothermic by 0.3-0.7 eV due to hy-

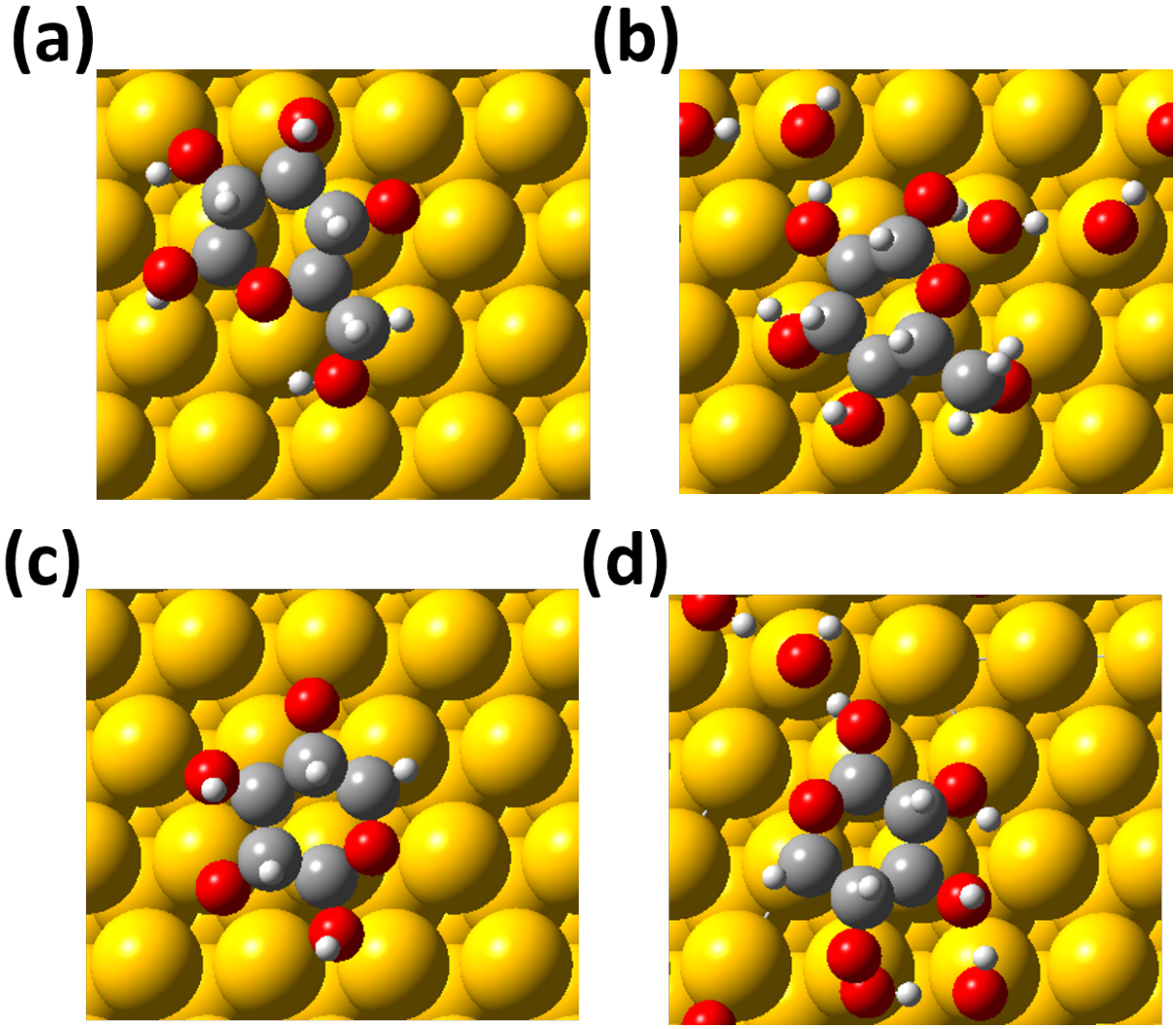

Figure 8: Adsorbed structures for (a) β-D-glucopyranose on bare Au(111), (b) on Au(111) + 1/4 ML OH, (c) β-D-xylose on bare Au(111), and (d) on Au(111) + 1/4 ML OH.

drogen bonding interactions with coadsorbed hydroxyl groups. Although hydrogen bonding interactions with surface water molecules are expected on both the bare and hydroxylated surface, these have been shown to be less influential proton abstractions than adsorbed oxide or hydroxide species.[60,61]

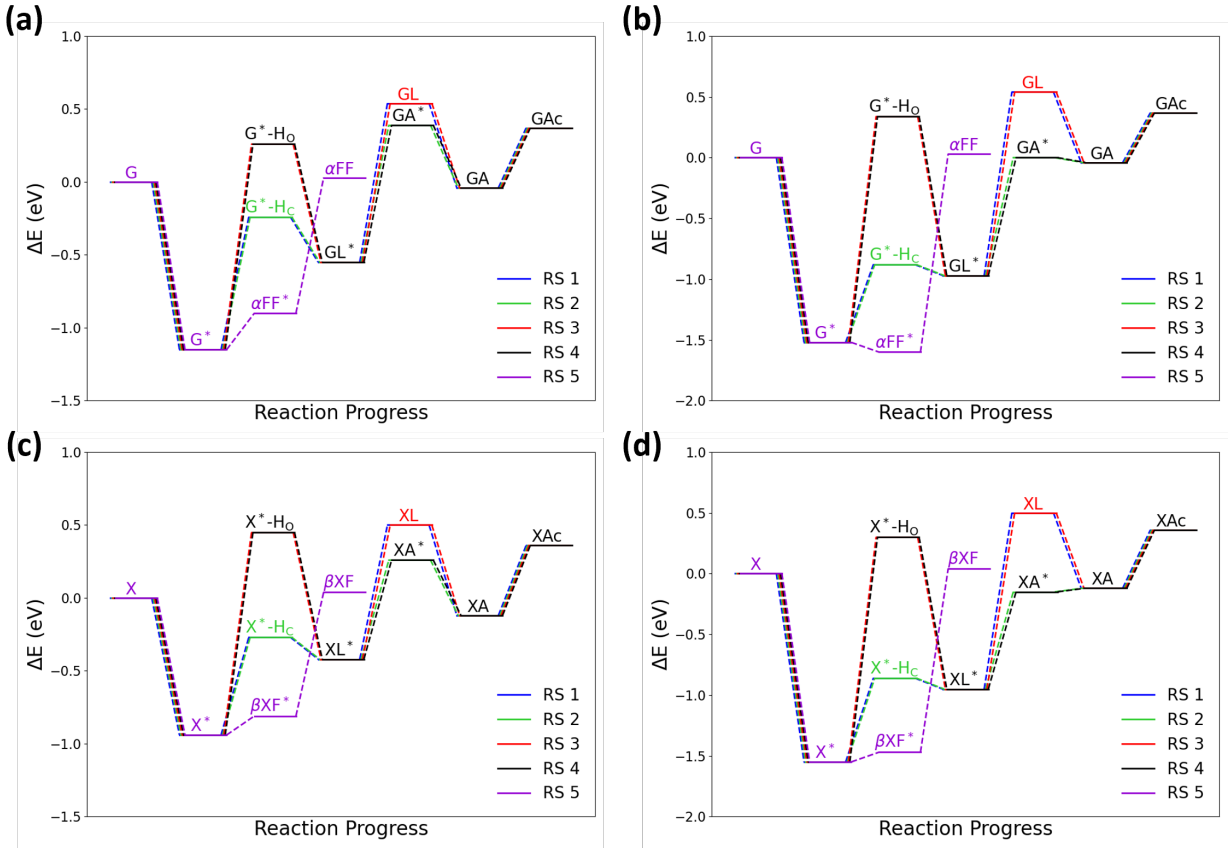

Figure 9: Thermodynamic profile for the electrooxidation of (a) β-D-glucopyranose on a clean Au(111) surface and (b) with 1/4 ML OH, and (c) β-D-xylopyranose on a clean Au(111) surface and (d) with 1/4 ML OH following reaction paths given in Figure 2. Adsorbed species are labelled with an asterisk. G, GL, GA, GAc, and αFF correspond to glucose, gluconolactone, gluconate, gluconic acid, and α-fructofuranose, respectively. Similarly, X, XL, XA, XAc, and βXF represent xylose, xylonolactone, xylonate, xylonic acid, and β-xylulofuranose, respectively. HO and HC indicate the atom from which the first hydrogen is removed.

As shown in Figure 9 and Figure SI-11, the first PCET of both cyclic tautomers of glucose and xylose occurs preferentially at the relevant CH group, rather than at the OH group regardless of whether the Au(111) surface is hydroxylated or not. While this contradicts previous studies examining glucose oxidation on gold,[22,62] the CH dehydrogenation being the

preferred initial PCET agrees with similar studies on glycerol.[30,63,64] Although the reaction energy decreases for the CH dehydrogenation of both glucose tautomers on the Au(111) + 1/4 ML OH surface, no significant change was observed for the same step involving β-D-xylopyranose. In contrast, no stable singly dehydrogenated form of α-D-xylopyranose was observed on the Au(111) + 1/4 ML OH surface, which may indicate that $\beta \rightarrow \alpha$ tautomerization is necessary for xylose oxidation to proceed. The reaction energy for the double PCET from α-D-xylopyranose to form xylonolactone is 0.31 eV while the equivalent reaction energy for the β anomer is 0.60 eV. Although the lactone is more strongly adsorbed on the hydroxylated surface than the bare surface, the second PCET step becomes less exothermic on the Au(111) + 1/4 ML OH surface. Indeed, the largest increase in reaction energy is observed for gluconolactone produced from singly dehydrogenated α-D-glucopyranose: -0.27 eV on clean Au(111) and 0.32 eV on Au(111) + 1/4 ML OH. The second PCET reaction energy for α-D-glucopyranose on the Au(111) + 1/4 ML OH surface is also only 0.10 eV more exothermic than the first PCET. This suggests that the hydroxylated surface forms a nearly ideal catalyst for the oxidation of α-D-glucopyranose towards adsorbed gluconolactone. The difference between the reaction energies for the first and second PCET of β-D-glucopyranose also decreases from 1.21 eV to 0.73 eV as the surface becomes hydroxylated. No such significant change is observed for β-D-xylopyranose which is expected to be the dominant anomer adsorbed on the hydroxylated surface. The more favourable adsorption energetics for α-D-glucopyranose compared to β-D-glucopyranose and both D-xylopyranose anomers combined with nearly ideal PCET reaction energies may explain the higher yields of gluconic acid compared to xylonic acid under basic conditions.

The first two PCET are common to both mechanisms gluconate or xylonate forms in the bulk solution or on the electrode's surface, therefore it is necessary to consider the following steps to determine the preferred reaction mechanism. Gluconate, xylonate, and the corresponding lactones are all stabilized on the hydroxylated Au(111) surface compared to the bare surface. Lactone desorption therefore becomes more endothermic as the gold surface

Table 5: Standard equilibrium, surface equilibrium and limiting potentials (V_{RHE}) for the oxidation of glucopyranose and xylopyranose. RS1 and RS2 refer to the reaction paths given in Figure 2.

	glucopyranose				xylopyranose			
	β-D		α-D		β-D		α-D	
	RS1	RS2	RS1	RS2	RS1	RS2	RS1	RS2
U_{eq}^{0}	−0.02	−0.02	−0.03	−0.03	−0.06	−0.06	−0.05	−0.05
U_{eq}^{surf} (clean)	0.51	0.30	0.47	0.23	0.40	0.26	0.32	0.14
U_{eq}^{surf} (1/4 ML OH)	0.51	0.27	0.57	0.37	0.47	0.30	0.37	0.15
U_L (clean)	0.94	0.91	0.94	0.73	0.68	0.67	0.78	0.78
U_L (1/4 ML OH)	0.97	0.64	0.97	0.42	0.80	0.69	0.80	0.15

becomes hydroxylated. This might suggest that the surface mediated formation of gluconate or xylonate is the energetically preferred mechanism. It is important to note, however, that the formation and desorption of adsorbed gluconate or xylonate is effectively an oxidation followed by a reduction which will become increasingly unfavourable as the absolute potential or pH increases (refer to Figures SI-12 and SI-13). In contrast, the lactone desorption and subsequent formation of gluconate or xylonate in the bulk solution constitute so-called chemical steps and their energetics are not expected to be significantly affected by changes in the electrode's absolute potential. Forming the adsorbed gluconate or xylonate from the corresponding lactone becomes the potential limiting step for both glucose anomers and β-D-xylopyranose on both bare and hydroxylated Au(111) surfaces as well as for α-D-xylopyranose on Au(111) + 1/4 ML OH surface. This reaction step is at least 0.5 eV more endothermic than the first PCET for the most reactive anomers, that is α-D-glucopyranose and α-D-xylopyranose. Furthermore, this step also involves the ring opening and as a result may be kinetically more hindered than the simple dehydrogenation in the first two PCET steps or the ring opening in solution. This mechanism is unlikely to be available until much higher potentials than needed for the solution phase lactone mechanism and then only for a small window of potentials as the final reduction necessary for the desorption would become increasingly energetically unfavourable (see Figures SI-12 and SI-13). The solution phase lactone mechanism is expected to be the preferred mechanism having lower limiting

potentials than further surface-mediated oxidation. This agrees with previous experimental results which indicated that the first PCET is the limiting step[22] as well as our own experimental results which show that the kinetics of glucose and xylose oxidation are governed by diffusion processes. Under our experimental conditions, where the potential is fixed at 1.30 V_{RHE}, gluconate and xylonate desorption is 0.26 eV and 0.12 eV more favourable than the corresponding lactones, respectively. This difference falls within the average solvation error of 0.24 eV,[40] therefore the two mechanisms may be active at this potential. The desorption energies for gluconate and gluconolactone compared to xylonate and xylonolactone respectively, are similar, therefore the significantly more favourable energetics for the adsorption of and first two PCET from α-D-glucopyranose in particular contribute to the higher TOF observed for glucose compared to xylose.

Figure 9 also compares the energies of glucose oxidation with the formation of α-D-fructofuranose and xylose oxidation with the formation of β-D-xylulofuranose. As shown in Table 4, these are expected to be the dominant fructose and xylulose tautomers on both the bare and hydroxylated Au(111) surfaces. The overall isomerization between solution phase sugars is nearly thermoneutral. The reaction energies show that isomerization between adsorbed sugars is thermodynamically preferred over the first PCET step. Indeed, the isomerization is exothermic for α-D-xylopyranose on both surfaces as well as for β-D-glucopyranose on the Au(111) + 1/4 ML OH surface. Despite the favorable energetics, the isomerization is not an electrochemical reaction and the corresponding reaction energies will be relatively unaffected by an applied potential. In addition, coadsorbed hydroxyl groups stabilize α-D-fructofuranose and β-D-xylulofuranose such that desorbing these sugars is no longer competitive with lactone desorption or further oxidation.

The thermodynamically preferred mechanism for both sugars on both surfaces involves deprotonating the relevant carbon first. In general, the presence of coadsorbed hydroxide groups lowers the thermodynamic barrier for this step. On both bare and hydroxylated surfaces, the mechanism forming adsorbed gluconate or xylonate is only available at higher

potentials than for the mechanism where the lactone desorbs. In addition, gluconate or xylonate desorption is effectively a reduction and potential-dependent thereby decreasing the range of potentials at which this mechanism can be active. The presence of OH_{ads} facilitates sugar adsorption and lowers the reaction energy of the first PCET which represents the potential limiting step in the desorbing lactone mechanism. Previous studies have also shown that OH_{ads} contributes to lowering the kinetic barriers of PCET steps.[30] Furthermore, lactone desorption becomes more favourable than the desorption of fructose or xylulose on Au(111) + 1/4 ML OH compared to the bare surface suggesting OH_{ads} also has a role in the selectivity towards the corresponding sugar acids.

Conclusions

In this work, the effects of reaction parameters on the electrocatalytic oxidation of glucose and xylose were studied employing a mesoporous carbon-supported Au nanocatalyst. Temperature studies demonstrate an optimal temperature for ECO can increase the rate of oxidation while preventing side product formation. Experimental results also indicate an optimal OH^- concentration drives glucose and xylose ECO reactions. Higher OH^- concentration (therefore, higher pH) resulted in lower ECO activity possibly due to fewer active sites available for sugar adsorption. Side reactions at higher temperature and pH mainly involve the aldose to ketose isomerization (e.g. glucose to fructose) and the formation of lower molecular weight carboxylic acids (e.g. formic, glycolic, formic acids). Our computational results demonstrate the role OH_{ads} has in the sugars' ECO and selectivity by stabilizing adsorbed sugars and lowering the reaction energy for the first PCET. Glucose adsorption is energetically more favourable than xylose, particularly for the most reactive glucose tautomer, α-D-glucopyranose thus explaining the higher TOF observed for glucose. Our results also indicate that although both may be active, the mechanism forming gluconate or xylonate should be available for a narrower window of potentials than the lactone

desorption mechanism. Potential programmed glucose and xylose ECO, intended to keep a high catalytic activity for Au during prolonged electrolysis, showed lower sugar conversions compared to ECO at a fixed potential. This indicates that minimal Au deactivation occurs at the working (static) potential of 1.3 V_{RHE} and therefore, would not require dynamic in-situ reactivation. The results obtained in this study demonstrate that by tuning reaction parameters such as temperature and pH sugar ECO can be accomplished over a carbon-supported Au nanocatalyst with low metal loading. This in turn provides a further basis for the electrochemical production of higher-value chemicals from biomass sources, a process that could utilize renewable energy for sustainable chemical production.

Supporting Information Available

The supporting information is available free of charge at ACS provided link. XYZ files of relevant optimized structures are available at

`https://doi.org/10.23729/cda503c4-b3d5-4db4-b5f7-98a8f7f88092`

Calculation of Au dispersion in the SC/Au catalyst, Determination of the electrochemically active surface area (ECSA) of the SC/Au catalyst, Structural filtering process, Figures of final GC-DFT obtained structures, Potential energy surfaces, Potential-dependent thermodynamics, Cyclic voltammetry-derived Arrhenius plots for glucose and xylose ECO, Fixed vs. cycled potential (PDF)

Acknowledgement

J.P.O, R.M.K, N.K., M.P., I.A, and H.G. were supported by the Tiina and Antti Herlin Foundation (Finland) under the FosToBioH2 (From fossil to biohydrogen in Finnish (bio)industry - utilizing electrocatalysis in Aqueous Phase Reforming of hemicelluloses) project at Åbo Akademi University, Finland. They would also like to thank the Electron Microscopy Lab-

oratory, Institute of Biomedicine, University of Turku, and Biocenter Finland for the TEM images, and the Wihuri Physical Laboratory, Department of Physics and Astronomy, University of Turku for the XRD analysis. L.L. would like to thank Dr Timo Weckman for helpful discussions about DockOnSurf. Computational resources were provided by the CSC-IT Center for Science, Espoo, Finland. L.L. and K.H. were supported by Academy of Finland grant No. 351583.

References

(1) BP Statistical Review of World Energy. **2016**,

(2) Mettler, M. S.; Vlachos, D. G.; Dauenhauer, P. J. Top ten fundamental challenges of biomass pyrolysis for biofuels. *Energy Environ. Sci.* **2012**, *5*, 7797–7809.

(3) Isikgor, F. H.; Becer, C. R. Lignocellulosic biomass: a sustainable platform for the production of bio-based chemicals and polymers. *Polym. Chem.* **2015**, *6*, 4497–4559.

(4) Nebreda, A. P.; Grénman, H.; Mäki-Arvela, P.; Eränen, K.; Hemming, J.; Willför, S.; Murzin, D. Y.; Salmi, T. Acid hydrolysis of O-acetyl-galactoglucomannan in a continuous tube reactor: a new approach to sugar monomer production. *Holzforschung* **2016**, *70*, 187–194.

(5) Lu, X.; Junghans, P.; Wärnå, J.; Hilpmann, G.; Lange, R.; Trajano, H.; Eränen, K.; Estel, L.; Leveneur, S.; Grénman, H. Hydrolysis of semi-industrial aqueous extracted xylan from birch (Betula pendula) employing commercial catalysts: kinetics and modelling. *J. Chem. Technol. Biotechnol.* **2022**, *97*, 130–139.

(6) Lu, X.; Junghans, P.; Weckesser, S.; Wärnå, J.; Hilpmann, G.; Lange, R.; Trajano, H.; Eränen, K.; Estel, L.; Leveneur, S.; Grénman, H. One flow through hydrolysis and hydrogenation of semi-industrial xylan from birch (betula pendula) in a continuous reactor—Kinetics and modelling. *Chem Eng Process* **2021**, *169*, 108614.

(7) Werpy, T. A.; Holladay, J. E.; White, J. F. Top Value Added Chemicals From Biomass: I. Results of Screening for Potential Candidates from Sugars and Synthesis Gas. **2004**,

(8) ACS Community: GCI Nexus Blog. *Top Value Added Chemicals: The Biobased Economy 12 Years Later*, 2017; `https://communities.acs.org/t5/GCI-Nexus-Blog/Top-Value-Added-Chemicals-The-Biobased-Economy-12-Years-Later/ba-p/15759`, Accessed: 2023-12-06.

(9) Machado, J. V.; da Silva, M. L. A.; Silva, C. L. S.; Correia, M. C. G.; da Silva Ruy, A. D.; Pontes, L. A. M. Catalysts and processes for gluconic and glucaric acids production: A comprehensive review of market and chemical routes. *Catal. Commun.* **2023**, *182*, 106740.

(10) Jin, D.; Ma, J.; Li, Y.; Jiao, G.; Liu, K.; Sun, S.; Zhou, J.; Sun, R. Development of the synthesis and applications of xylonic acid: A mini-review. *Fuel* **2022**, *314*, 122773.

(11) Rafaïdeen, T.; Baranton, S.; Coutanceau, C. Highly efficient and selective electrooxidation of glucose and xylose in alkaline medium at carbon supported alloyed PdAu nanocatalysts. *Appl. Catal. B* **2019**, *243*, 641–656.

(12) Onda, A.; Ochi, T.; Kajiyoshi, K.; Yanagisawa, K. A new chemical process for catalytic conversion of d-glucose into lactic acid and gluconic acid. *Appl. Catal. A: Gen.* **2008**, *343*, 49–54.

(13) Tathod, A.; Kane, T.; Sanil, E.; Dhepe, P. L. Solid base supported metal catalysts for the oxidation and hydrogenation of sugars. *J Mol Catal A Chem* **2014**, *388-389*, 90–99, Special Issue on Biomass Catalysis.

(14) Liang, X.; Liu, C.-j.; Kuai, P. Selective oxidation of glucose to gluconic acid over argon plasma reduced Pd/Al2O3. *Green Chem.* **2008**, *10*, 1318–1322.

(15) Cattaneo, S.; Stucchi, M.; Villa, A.; Prati, L. Gold Catalysts for the Selective Oxidation of Biomass-Derived Products. *ChemCatChem* **2019**, *11*, 309–323.

(16) Brouzgou, A.; Tsiakaras, P. Electrocatalysts for Glucose Electrooxidation Reaction: A Review. *Topics in Catalysis* **2015**, *58*, 1311–1327.

(17) Moggia, G.; Schalck, J.; Daems, N.; Breugelmans, T. Two-steps synthesis of D-glucaric acid via D-gluconic acid by electrocatalytic oxidation of D-glucose on gold electrode: Influence of operational parameters. *Electrochim. Acta* **2021**, *374*, 137852.

(18) Holade, Y.; Servat, K.; Napporn, T. W.; Morais, C.; Berjeaud, J.-M.; Kokoh, K. B. Highly Selective Oxidation of Carbohydrates in an Efficient Electrochemical Energy Converter: Cogenerating Organic Electrosynthesis. *ChemSusChem* **2016**, *9*, 252–263.

(19) Adzic, R.; Hsiao, M.; Yeager, E. Electrochemical oxidation of glucose on single crystal gold surfaces. *J. electroanal. chem. interfacial electrochem.* **1989**, *260*, 475–485.

(20) Oña, J. P.; Latonen, R.-M.; Kumar, N.; Peurla, M.; Angervo, I.; Grénman, H. Electrocatalytic hydrogenation and oxidation of glucose and xylose on mesoporous carbon-supported Au nanocatalysts. *Electrochim. Acta* **2023**, *437*, 141536.

(21) Fenelonov, V.; Likholobov, V.; Derevyankin, A.; Mel'gunov, M. Porous carbon materials prepared from C1–C3 hydrocarbons. *Catal. Today* **1998**, *42*, 341–345.

(22) Holade, Y.; Guesmi, H.; Filhol, J.-S.; Wang, Q.; Pham, T.; Rabah, J.; Maisonhaute, E.; Bonniol, V.; Servat, K.; Tingry, S.; Cornu, D.; Kokoh, K. B.; Napporn, T. W.; Minteer, S. D. Deciphering the Electrocatalytic Reactivity of Glucose Anomers at Bare Gold Electrocatalysts for Biomass-Fueled Electrosynthesis. *ACS Catal.* **2022**, *12*, 12563–12571.

(23) Belgsir, E.; Bouhier, E.; Essis Yei, H.; Kokoh, K.; Beden, B.; Huser, H.; Leger, J.-M.;

Lamy, C. Electrosynthesis in aqueous medium: a kinetic study of the electrocatalytic oxidation of oxygenated organic molecules. *Electrochim. Acta* **1991**, *36*, 1157–1164.

(24) Pfisterer, J. H. K.; Nattino, F.; Zhumaev, U. E.; Breiner, M.; Feliu, J. M.; Marzari, N.; Domke, K. F. Role of OH Intermediates during the Au Oxide Electro-Reduction at Low pH Elucidated by Electrochemical Surface-Enhanced Raman Spectroscopy and Implicit Solvent Density Functional Theory. *ACS Catal.* **2020**, *10*, 12716–12726.

(25) Strobl, J. R.; Scherson, D. The adsorption of perchlorate, sulfate, selenate and water on Au(111)-textured electrodes from aqueous solutions: Simultaneous voltammetric, optical and microgravimetric studies. *Electrochim. Acta* **2021**, *394*, 139107.

(26) Zhumaev, U.; Rudnev, A. V.; Li, J.-F.; Kuzume, A.; Vu, T.-H.; Wandlowski, T. Electro-oxidation of Au(111) in contact with aqueous electrolytes: New insight from in situ vibration spectroscopy. *Electrochim. Acta* **2013**, *112*, 853–863.

(27) Franks, F. Physical chemistry of small carbohydrates - equilibrium solution properties. *Pure Appl. Chem.* **1987**, *59*, 1189–1202.

(28) Schmidt, R. K.; Karplus, M.; Brady, J. W. The Anomeric Equilibrium in d-Xylose: Free Energy and the Role of Solvent Structuring. *J. Am. Chem. Soc.* **1996**, *118*, 541–546.

(29) Miyata, T. Reference Interaction Site Model Study on the Anomeric Equilibrium of D-Glucose in Aqueous Solution. *Condens Matter Phys* **2007**, *10*, 433.

(30) Verma, A. M.; Laverdure, L.; Melander, M. M.; Honkala, K. Mechanistic Origins of the pH Dependency in Au-Catalyzed Glycerol Electro-oxidation: Insight from First-Principles Calculations. *ACS Catal.* **2022**, *12*, 662–675.

(31) Martí, C.; Blanck, S.; Staub, R.; Loehlé, S.; Michel, C.; Steinmann, S. N. DockOnSurf: A Python Code for the High-Throughput Screening of Flexible Molecules Adsorbed on Surfaces. *J Chem Inf Model* **2021**, *61*, 3386–3396.

(32) Mortensen, J. J.; Hansen, L. B.; Jacobsen, K. W. Real-space grid implementation of the projector augmented wave method. *Phys. Rev. B* **2005**, *71*, 035109.

(33) Enkovaara, J. et al. Electronic structure calculations with GPAW: a real-space implementation of the projector augmented-wave method. *J. Phys. Condens. Matter* **2010**, *22*, 253202.

(34) Melander, M. M.; Kuisma, M. J.; Christensen, T. E. K.; Honkala, K. Grand-canonical approach to density functional theory of electrocatalytic systems: Thermodynamics of solid-liquid interfaces at constant ion and electrode potentials. *J. Chem. Phys.* **2018**, *150*, 041706.

(35) Kastlunger, G.; Lindgren, P.; Peterson, A. A. Controlled-Potential Simulation of Elementary Electrochemical Reactions: Proton Discharge on Metal Surfaces. *J. Phys. Chem. C* **2018**, *122*, 12771–12781.

(36) Held, A.; Walter, M. Simplified continuum solvent model with a smooth cavity based on volumetric data. *J. Chem. Phys.* **2014**, *141*, 174108.

(37) Perdew, J. P.; Burke, K.; Ernzerhof, M. Generalized Gradient Approximation Made Simple. *Phys. Rev. Lett.* **1996**, *77*, 3865–3868.

(38) Tkatchenko, A.; Scheffler, M. Accurate Molecular Van Der Waals Interactions from Ground-State Electron Density and Free-Atom Reference Data. *Phys. Rev. Lett.* **2009**, *102*, 073005.

(39) Al-Saidi, W. A.; Voora, V. K.; Jordan, K. D. An Assessment of the vdW-TS Method for Extended Systems. *J. Chem. Theory Comput.* **2012**, *8*, 1503–1513.

(40) Heenen, H. H.; Gauthier, J. A.; Kristoffersen, H. H.; Ludwig, T.; Chan, K. Solvation at metal/water interfaces: An ab initio molecular dynamics benchmark of common computational approaches. *J. Chem. Phys.* **2020**, *152*, 144703.

(41) Davey, W. P. Precision Measurements of the Lattice Constants of Twelve Common Metals. *Phys. Rev.* **1925**, *25*, 753–761.

(42) Pasta, M.; La Mantia, F.; Cui, Y. Mechanism of glucose electrochemical oxidation on gold surface. *Electrochim. Acta* **2010**, *55*, 5561–5568.

(43) Moggia, G.; Kenis, T.; Daems, N.; Breugelmans, T. Electrochemical Oxidation of d-Glucose in Alkaline Medium: Impact of Oxidation Potential and Chemical Side Reactions on the Selectivity to d-Gluconic and d-Glucaric Acid. *ChemElectroChem* **2020**, *7*, 86–95.

(44) Pasta, M.; Ruffo, R.; Falletta, E.; Mari, C. M.; Pina, C. D. Alkaline glucose oxidation on nanostructured gold electrodes. *Gold Bull* **2010**, *43*, 57–64.

(45) Yei, L.; Beden, B.; Lamy, C. Electrocatalytic oxidation of glucose at platinum in alkaline medium: on the role of temperature. *J. electroanal. chem. interfacial electrochem.* **1988**, *246*, 349–362.

(46) Holade, Y.; Hebié, S.; Maximova, K.; Sentis, M.; Delaporte, P.; Kokoh, K. B.; Napporn, T. W.; Kabashin, A. V. Bare laser-synthesized palladium–gold alloy nanoparticles as efficient electrocatalysts for glucose oxidation for energy conversion applications. *Catal. Sci. Technol.* **2020**, *10*, 7955–7964.

(47) Brouzgou, A.; Yan, L.; Song, S.; Tsiakaras, P. Glucose electrooxidation over PdxRh/C electrocatalysts in alkaline medium. *Appl. Catal. B* **2014**, *147*, 481–489.

(48) Holade, Y.; Both Engel, A.; Tingry, S.; Cherifi, A.; Cornu, D.; Servat, K.; Napporn, T. W.; Kokoh, K. B. Insights on Hybrid Glucose Biofuel Cells Based on Bilirubin Oxidase Cathode and Gold-Based Anode Nanomaterials. *ChemElectroChem* **2014**, *1*, 1976–1987.

(49) Danilov, F. I.; Protsenko, V. S. Actual activation energy of electrochemical reactions at stage charge transfer. *Russ. J. Electrochem.* **2010**, *46*, 188–195.

(50) Ghosh, S.; Holade, Y.; Remita, H.; Servat, K.; Beaunier, P.; Hagège, A.; Kokoh, K. B.; Napporn, T. W. One-pot synthesis of reduced graphene oxide supported gold-based nanomaterials as robust nanocatalysts for glucose electrooxidation. *Electrochim. Acta* **2016**, *212*, 864–875.

(51) Holade, Y.; Engel, A. B.; Servat, K.; Napporn, T. W.; Morais, C.; Tingry, S.; Cornu, D.; Kokoh, K. B. Electrocatalytic and Electroanalytic Investigation of Carbohydrates Oxidation on Gold-Based Nanocatalysts in Alkaline and Neutral pHs. *J Electrochem Soc* **2018**, *165*, H425.

(52) Hebié, S.; Holade, Y.; Maximova, K.; Sentis, M.; Delaporte, P.; Kokoh, K. B.; Napporn, T. W.; Kabashin, A. V. Advanced Electrocatalysts on the Basis of Bare Au Nanomaterials for Biofuel Cell Applications. *ACS Catal.* **2015**, *5*, 6489–6496.

(53) Hebié, S.; Cornu, L.; Napporn, T. W.; Rousseau, J.; Kokoh, B. K. Insight on the Surface Structure Effect of Free Gold Nanorods on Glucose Electrooxidation. *J. Phys. Chem. C* **2013**, *117*, 9872–9880.

(54) Hsiao, M.; Adzic, R.; Yeager, E. The effects of adsorbed anions on the oxidation of D-glucose on gold single crystal electrodes. *Electrochim. Acta* **1992**, *37*, 357–363.

(55) Tung, S.-P.; Huang, T.-K.; Lee, C.-Y.; Chiu, H.-T. Electrochemical growth of gold nanostructures on carbon paper for alkaline direct glucose fuel cell. *RSC Adv.* **2012**, *2*, 1068–1073.

(56) Jaseja, M.; Perlin, A. S.; Dais, P. Two-dimensional NMR spectral study of the tautomeric equilibria of D-fructose and related compounds. *Magn Reson Chem* **1990**, *28*, 283–289.

(57) Hyvönen, L.; Varo, P.; Koivistoinen, P. Tautomeric Equilibria of D-Glucose AND D-Fructose: Polarimetric Measurements. *J. Food Sci.* **1977**, *42*, 652–653.

(58) Barclay, T.; Ginic-Markovic, M.; Johnston, M. R.; Cooper, P.; Petrovsky, N. Observation of the keto tautomer of d-fructose in D2O using 1H NMR spectroscopy. *Carbohydr. Res.* **2012**, *347*, 136–141.

(59) Wu, J.; Serianni, A. S.; Vuorinen, T. Furanose ring anomerization: kinetic and thermodynamic studies of the d-2-pentuloses by 13C-n.m.r. spectroscopy. *Carbohydr. Res.* **1990**, *206*, 1–12.

(60) Chang, C.-R.; Yang, X.-F.; Long, B.; Li, J. A Water-Promoted Mechanism of Alcohol Oxidation on a Au(111) Surface: Understanding the Catalytic Behavior of Bulk Gold. *ACS Catal.* **2013**, *3*, 1693–1699.

(61) Behravesh, E.; Melander, M. M.; Wärnå, J.; Salmi, T.; Honkala, K.; Murzin, D. Y. Oxidative dehydrogenation of ethanol on gold: Combination of kinetic experiments and computation approach to unravel the reaction mechanism. *J Catal* **2021**, *394*, 193–205.

(62) Wei, L.; Sheng, T.; Ye, J.-Y.; Lu, B.-A.; Tian, N.; Zhou, Z.-Y.; Zhao, X.-S.; Sun, S.-G. Seeds and Potentials Mediated Synthesis of High-Index Faceted Gold Nanocrystals with Enhanced Electrocatalytic Activities. *Langmuir* **2017**, *33*, 6991–6998.

(63) Garcia, A. C.; Kolb, M. J.; van Nierop y Sanchez, C.; Vos, J.; Birdja, Y. Y.; Kwon, Y.; Tremiliosi-Filho, G.; Koper, M. T. M. Strong Impact of Platinum Surface Structure on Primary and Secondary Alcohol Oxidation during Electro-Oxidation of Glycerol. *ACS Catal.* **2016**, *6*, 4491–4500.

(64) Liu, B.; Greeley, J. Decomposition Pathways of Glycerol via C–H, O–H, and C–C Bond Scission on Pt(111): A Density Functional Theory Study. *J. Phys. Chem. C* **2011**, *115*, 19702–19709.

TOC Graphic

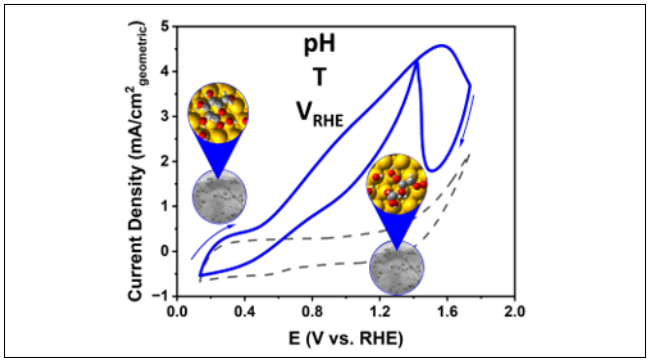
pH
T
V_{RHE}
Current Density (mA/cm^2 geometric)
E (V vs. RHE)
5
4
3
2
1
0
−1
0.0
0.4
0.8
1.2
1.6
2.0